Carbon 229 (2024) 119550

Contents lists available at ScienceDirect

Carbon

journal homepage: www.elsevier.com/locate/carbon

Design and optimization of an electrochemical sensor based on carbon nanotubes for the reliable voltammetric detection of serotonin in complex biological fluids

Giuseppe Misia [a], Claudio Evangelisti [b], Juan P. Merino [c], Emanuela Pitzalis [b], Adrián M. Abelairas [c], Jesús Mosquera [c], Alejandro Criado [c], Maurizio Prato [a,d,e], Alessandro Silvestri [f,*]

[a] Department of Chemical and Pharmaceutical Sciences, Università Degli Studi di Trieste, Trieste, 34127, Italy
[b] Institute of Chemistry of Organometallic Compounds, CNR-ICCOM, 56124, Pisa, Italy
[c] Centro Interdisciplinar de Química e Bioloxía (CICA) and Departamento de Química, Facultade de Ciencias, Universidade da Coruña, 15071, A Coruña, Spain
[d] Center for Cooperative Research in Biomaterials (CIC BiomaGUNE), Basque Research and Technology Alliance (BRTA), Paseo de Miramon 194, 20014, Donostia-San Sebastián, Spain
[e] Ikerbasque Basque Foundation for Science Bilbao, 48009, Spain
[f] Department of Molecular Sciences and Nanosystems, Ca' Foscari University of Venice, Venezia, 30170, Italy

ARTICLE INFO

Keywords:
Serotonin
Electrochemical sensor
Differential pulsed voltammetry (DPV)
Carbon nanotubes (CNT)
Gold nanoparticles (Au NPs)
Metal vapor synthesis (MVS)
Molecular imprinted polymers (MIP)
Design of experiment (DoE)

ABSTRACT

Serotonin concentration in peripherical biological fluids is correlated with the insurgence of several pathologies and represents valuable information on the human physical and mental state of health. Rapid, portable, and reliable electrochemical sensors can mine this useful information in real-time and *in situ*. However, the main challenge that hampers their implementation is the poor operational stability in biological fluids rich in biomacromolecules, which can induce the fouling of the electrode altering or invalidating the analytical performance of the sensor. Herein, we propose the design of a reliable and robust voltammetric sensor for detecting serotonin in plasma. The sensor is based on multiwall carbon nanotubes modified with ligand-free gold nanoparticles obtained by metal vapor synthesis, which can efficiently catalyze the oxidation of serotonin. A thin layer of molecular imprinted polymer is added to provide selectivity and antifouling properties to the sensor. By applying a design of the experiment, to optimize the experimental condition of the differential pulsed voltammetry, and adsorptive stripping to selectively pre-accumulate serotonin in the artificial receptor, we achieved serotonin detection in plasma with sensitivity (6.7 μA μmol L^{-1} cm^{-2}) and limits of detection (1.0 μmol L^{-1}) comparable to those registered in phosphate buffer solution.

1. Introduction

Serotonin, also known as 5-hydroxytryptamine (5-HT), is a small molecule that acts both as a neurotransmitter in the central nervous system and as a hormone in the periphery of our bodies. Due to this dual nature, 5-HT biological function is complex, involving diverse physiological functions such as sleep, cognition, learning, memory, reward processing, aggressiveness, appetite, and sexual behavior. 5-HT, as a hormone, is also implicated in non-neuronal processes like the regulation of cardiovascular activity, vasoconstriction, vasodilation, glucose homeostasis, and metabolism [1,2]. Being such a ubiquitous biomolecule, 5-HT is an extremely interesting biomarker for several pathologies [3,4]. Indeed, it has been demonstrated that high concentrations of 5-HT can be related to autism spectrum disorder [5], carcinoid syndrome [6], and coronary artery disease [7]. In contrast, a decrease in the physiological concentration of 5-HT can be indicative of attention deficit hyperactivity disorder [8,9], kidney diseases, and diabetes [10].

Even though 100 years passed since the discovery of serotonin, several of its physiological functions remain elusive, and its involvement in some pathological conditions such as mental depression [11,12], and communicative diseases [13–16] is still controversial [17].

* Corresponding author. Department of Molecular Sciences and Nanosystems, Ca' Foscari University of Venice, Venezia, 30170, Italy
E-mail addresses: prato@units.it (M. Prato), alessandro.silvestri@unive.it (A. Silvestri).

https://doi.org/10.1016/j.carbon.2024.119550
Received 13 July 2024; Received in revised form 10 August 2024; Accepted 13 August 2024
Available online 15 August 2024

The possibility of measuring in real-time the concentration of serotonin in peripheral biological fluids could allow us to investigate the more elusive physiological functions of 5-HT and solve several controversies around this molecule. Furthermore, rapid, portable, and reliable technologies for serotonin detection could also help emergency clinicians in the timely diagnosis and management of serotonin fatal syndrome [18], a rare drug-induced clinical condition, with a mortality of 50 % within 24 h from the onset of the symptoms [19].

There are various instrumental approaches for the detection of serotonin. High-performance liquid chromatography (HPLC), coupled with mass spectrometry (MS), is among the most used analytical techniques for the analysis of 5-HT and its metabolites, constituting a powerful tool with high selectivity and sensitivity [20–22]. However, HPLC-MS requires analytical laboratories to be performed and is not a suitable solution for rapid and *in situ* measurements or continuous monitoring of 5-HT levels.

An electrochemical sensor instead can be easily miniaturized to determine the concentration of 5-HT in a few seconds, exploiting the current generated by the oxidation reaction of serotonin. The main challenge hampering the direct electrochemical detection of serotonin is imposed by biological fluids. Indeed, serotonin can be found in the peripheral biological fluids in various concentrations. 5-HT levels can range from 0.1 to 0.7 μmol L^{-1} in urines [23], from 0.3 to 2 μmol L^{-1} in blood serum [21,24] and from 0.5 to 20 μmol L^{-1} in saliva [25]. However, in these complex biological matrices, several problems arise, like the presence of interfering species, which can disturb the electrochemical response affecting the selectivity of the sensor, the fouling generated by proteins and other bio-macromolecules that can modify the surface of the electrode, and the complex oxidation mechanism of serotonin that can generate several subproducts affecting the detection [26]. These open challenges make the 5-HT electrochemical detection still a very timely topic [27,28].

Indeed, Xu et al. recently published an electrochemical sensor for detecting 5-HT in human serum based on carbon spheres decorated with ultrafine Fe_3O_4 nanoparticles, which exhibit excellent sensing performance [29]. Kanbaca et al. proposed a disposable electrochemical sensor for the simultaneous determination of dopamine (DA) and 5-HT in blood serum. This sensor has been designed by modifying screen-printed carbon electrodes (SPCE) with titanium oxide nanoparticles and electrodeposited Au NPs. Finally, a deep eutectic solvent was used to electro-polymerize Nile blue on the nanostructured electrode [30]. Another recent work aiming at the detection of 5-HT in bodily fluids has been recently published by Liu et a., in which the authors exploited electrodes modified with vertical graphene co-doped with boron and nitrogen to detect 5-HT in gastric, intestine juices, and blood samples [31]. Finally, Wu et al. developed a sensitive electrochemical sensor utilizing ferrocene covalently linked gold nanoparticles on multiwall carbon nanotubes (MWCNTs) for 5-HT detection in urines [32].

Herein, we exploited the advantage of MWCNTs to improve both the electron transfer and the mass transfer kinetics in 5-HT electrochemical sensors [33]. Thanks to this peculiar property, CNTs have been identified as an optimal material for detecting electroactive neurotransmitters, providing higher peaks with narrower full width at medium height (FWHM), and therefore improving the sensitivity and selectivity of the voltammetric detection [33]. Moreover, it is possible to tune their properties by introducing multiple moieties on their surface, opening to infinite possible combinations for sensor manufacture.

In this work, we propose a novel design for a highly performing and robust voltammetric sensor (based on differential pulsed voltammetry, DPV) for the detection of 5-HT, able to operate in complex matrixes enriched with bio-macromolecules and interferents such as plasma. To further improve the electrocatalytic properties of the MWCNTs, we decorated them with size-controlled gold nanoparticles (Au NPs) obtained by metal vapor synthesis (MVS). These pre-formed NPs, herein used for the first time in an electrochemical sensor, contain only metal in its reduced form and they are weakly stabilized only by the solvent used in the synthesis without the presence of additional ligands (i.e. molecular or polymeric) [34]. These properties, together with the small size and the vast exposed surface makes these particles optimal catalysts [35–38] and electrocatalysts [39]. To achieve a stable and controlled anchoring of MVS-derived Au NPs on MWCNTs we exploited the covalent chemical modification of carbon nanotubes using a sulfur-bearing aryl diazonium salt (4,4′-dithiodibenzenediazonium tetrafluoroborate, $DTDBBF_4$). This approach involves a single electron transfer reaction between MWCNTs and the corresponding diazonium salt, followed by a radical addition that modifies the carbon nanotube with a phenyl group. Subsequently, the generated phenyl radicals react with phenyl groups on the nanotube surface, creating polymer chains. The proposed functionalization strategy allows the protection of the thiol from possible side reactions during the covalent chemical modification while controlling the oligomerization degree through a reductive cleavage of the disulfide bond in the final step of the functionalization. We completed the design of the electrode by electropolymerizing a molecularly imprinted polymer (MIP) selective serotonin on top of the modified electrode, improving the selectivity and conferring antifouling properties to the system. Finally, we demonstrated that by recurring to a design of the experiment (DoE) to optimize the DPV parameters and by performing an electrically driven accumulation of 5-HT inside the MIP it is possible to maximize the analytical parameters of the sensor such as limit of detection (LOD) and sensitivity.

2. Materials and methods

MWCNTs were purchased from Nanostructured & Amorphous Materials Inc. And purified as described in section 2.3. 4-Aminothiophenol was purchased from TCI chemicals and used without further purification. All other reagents were purchased from Sigma Aldrich and used without further purification.

^{1}H NMR spectra were registered with a Varian 400 MHz spectrometer (^{1}H: 400 MHz, ^{19}F: 376 MHz, ^{13}C: 101 MHz). Fourier transform infrared spectroscopy (FT-IR) spectra were registered using a Bruker Invenio-X in an attenuated total reflectance (ATR) mode with diamond crystal.

Differential Scanning Calorimetry (DSC) measurements were performed on Discovery DSC 250 (TA Instruments), where 2.6 mg of $DTDBBF_4$ were weighed in a Tzero Aluminium Hermetic pan and were heated from 25 °C to 250 °C, with a ramp of 5 °C min^{-1}.

Thermogravimetric analysis (TGA) measurements were carried out with a TGA Discovery (TA Instruments), where 0.5 mg of material were weighed in a Platinum HT pan and heated in N_2 atmosphere (for MWCNTs, disulphide-functionalized MWCNTs, MWCNT-SS, and thiol-functionalized MWCNTs, MWCNT-SH) or air (for MWCNTs and gold-nanoparticles-functionalized MWCNTs, MWCNT-S-Au). First, an isotherm at 100 °C was applied for 20 min. Subsequently, the samples were heated to 800 °C with a ramp of 10 °C min^{-1}.

X-ray Photoelectron Spectroscopy (XPS) spectra were registered with an XPS/UPS – SPECS SAGE HR-100 equipped with a 100 mm radius PHOIBOS analyzer, where 421 Mg Kα X-ray source was used. The samples were prepared by drop-casting 80 μL of a 0.5 mg mL^{-1} suspension of material in Milli-Q water, on a gold-coated substrate (for MWCNTs, MWCNT-SS, MWCNT-SH) or silicon oxide substrate (for MWCNT-S-Au). The samples were left to dry under reduced pressure. The spectra were fitted using CasaXPS. Calibration was performed using the major component of the C high-resolution spectrum as a reference at 284.5 eV, which is the value reported for sp^2 carbon for CNTs [40].

For inductively coupled plasma optical emission spectrometry (ICP-OES, PerkinElmer Optima 8000), the metal-containing acetone solution (0.5 mL) was heated over a heating plate in a porcelain crucible, in the presence of aqua regia (2 mL), four times. The solid residue was dissolved in 0.5 mol L^{-1} aqueous HCl and diluted with de-ionized water to a final volume of 50 mL.

For inductively coupled plasma mass spectrometry (ICP-MS) analysis, Thermo Fisher iCap-Q, equipped with a He gas kinetic energy discrimination (KED) collision/reaction cell, was used. MWCNT-S-Au were digested in 2 mL of a HCl/HNO_3 (1:3) mixture, in a microwave digestor, applying a ramp of temperature of 10 °C min^{-1} from 25 °C to 200 °C. The obtained solution was diluted to 10 mL with Milli-Q water, before the analysis.

Transmission electron microscopy (TEM) micrographs were obtained with a JEOL JEM-1400 PLUS transmission electron microscope equipped with a GATAN US1000 CCD camera, operating at an acceleration voltage of 120 kV. The samples were prepared by drop-casting 5 μL a 0.1 mg mL^{-1} suspension of material on carbon film 300 mesh copper grids, purchased from Electron Microscopy Sciences. The statistical dimensional analysis was performed over 970 Au NPs with Fiji software.

All electrochemical measurements were performed using an electrochemical workstation Autolab MSTAT204 potentiostat/galvanostat (Metrohm Autolab) interfaced to a PC with Nova 2.1.6 software, at laboratory room temperature (25 °C). Commercially available SPCEs (DRP 110, provided by Metrohm Dropsens) were used to study the electrocatalytic activity of MWCNT-S-Au and to manufacture the final sensor, SPCE/MWCNT-S-Au/MIP.

Scanning electron microscopy (SEM) images were obtained using JSM7200F JEOL at 3–10 kV. For the characterization of Gold NPs, a lower electron detector (LED) was used instead of the upper secondary electron detector (USD). SEM images were acquired from the corresponding samples without previous treatment.

2.1. Synthesis of 4,4′-dithiodibenzenediazonium tetrafluoroborate

To synthesize 4,4′-dithiodibenzenediazonium tetrafluoroborate ($DTDBBF_4$), first 4-aminothiophenol (ATP) was oxidized to dithiodianiline (DTDA). 2 g of ATP were dissolved in 300 mL of H_2O/EtOH (1:1) mixture, then 1.25 eq of H_2O_2 and 0.15 eq of NH_3 were added to the solution, which was left stirring at room temperature for 2 h. DTDA was extracted with DCM and washed twice with H_2O. Finally, the organic phase was dried over Na_2SO_4 and the solvent was evaporated to isolate the product. DTDA was obtained with a quantitative yield and characterized by ^1H NMR. (DMSO-d_6, δ = 7.06 (m, 4H), 6.56 (m, 4H), 5.49 (s, 4H))

Subsequently, the obtained DTDA was dissolved in 60 mL of glacial acetic acid and 12 mL of HBF_4 were added. While stirring, 6 mL of isopentyl nitrite were added dropwise. The mixture was left stirring for 45 min, then 100 mL of Et2O were poured into the reaction mixture, and the flask was stored at −20 °C overnight. Finally, $DTDBBF_4$ was isolated by filtration and characterized by ^1H NMR (DMSO-d_6, δ = 8.61 (m, 4H), 8.14 (m, 4H)) and ATR-FTIR (2264 cm^{-1}(N≡ N), 1552 cm^{-1}(Aromatic C═C), 1054 cm^{-1}(BF_4^-), 521 cm^{-1}(S–S)) [41].

2.2. Metal vapor synthesis of Au NPs

In a typical experiment, Au vapors, generated at 10^{-5} mBar by resistive heating of the metal (100 mg of Au chips) in an alumina-coated tungsten crucible, were co-condensed at liquid nitrogen temperature (−196 °C) with acetone (100 mL) in the glass reactor chamber of a previously described MVS reactor [34] for 1 h. The reactor chamber was then heated to the melting point of the solid matrix (ca. − 95 °C), and the resulting deep purple solution (95 mL) was siphoned and handled at low temperature (−20 °C) with the Schlenk tube technique. The gold content of the acetone solution was calculated from ICP-OES and resulted in 0.57 mg mL^{-1}.

2.3. Synthesis of MWCNT-S-Au

MWCNTs were first purified, by sonication in 6 mol L^{-1} HCl for 6 h in a sonicating bath, then recovered by filtration and washed with Milli-Q water until neutral pH was reached. The XPS confirmed that they are mainly composed of C (96.80 %) with a low degree of O (3.20 %). The survey and high-resolution spectra of the purified MWCNTs confirmed the absence of contaminations by Fe and other metals (Fig. S4).

MWCNTs were functionalized by a radical reaction with the previously synthesized $DTDBBF_4$. 60 mg of MWCNTs were suspended in 60 mL of dimethylformamide (DMF), by sonicating for 5 min in a sonicating bath. The suspension was heated at 80 °C and 1.114 g (0.5 eq for each carbon atom) of $DTDBBF_4$ were added. The mixture was left stirring overnight and the product, MWCNT-SS, was isolated by filtration, washing twice with DMF and EtOAc.

To obtain the final MWCNT-SH, MWCNT-SS were reduced with tris (2-carboxyethyl)phosphine (TCEP). A solution was prepared by dissolving 250 mg of TCEP in 50 mL of phosphate buffer solution at pH = 7. 50 mg of MWCNT-SS were then dispersed in 50 mL of Milli-Q water by sonicating for 5 min and the TCEP was added. The mixture was left to stir overnight and finally, the product was isolated by filtration washing with 1 L of Milli-Q water.

Au NPs-acetone solution (was then added to a suspension containing the MWCNT-SH (or MWCNT-SS) (50 mg) in acetone (5 mL). The mixture was stirred overnight at 25 °C. The Au NPs solution was removed and the solid was washed with *n*-pentane (3 × 10 mL) and dried under reduced pressure.

2.4. Electrochemical characterization of MWCNT-S-Au

The electrocatalytic activity of MWCNT-S-Au was evaluated by Linear Sweep Voltammetry (LSV). 10 μL of a 0.5 mg mL^{-1} suspension of MWCNT-S-Au were drop-casted on the surface of the working electrode of an SPCE. Upon drying, 60 μL of a 12 μ mol L^{-1} solution of 5-HT in phosphate buffer (PBS) 0.1 mol L^{-1} and KCl 0.1 mol L^{-1} (pH = 7.0) were cast on the surface of the SPCE/MWCNT-S-Au and LSV was carried out by scanning applied potential from 0.1 to 0.4 V, with a scan rate of 20 mV s^{-1}.

Cyclic Voltammetry (CV) was used to study the mechanism of oxidation of 5-HT at the interface. The applied potential was scanned from 0 to 0.5 V, at different scan rates, ranging from 20 to 65 mV s^{-1}.

2.5. Design of the experiment

DPV was used to perform sensing of 5-HT. The applied potential was scanned from 0.1 to 0.4 V, with a step potential of 5 mV and an interval time (IT) of 250 ms. The baseline was subtracted from the obtained voltammograms with a moving average baseline model. Modulation time (MT) and modulation amplitude (MA) were optimized by DoE [42].

A factorial design was applied, where 3 equally spaced levels (low, medium, and high) were chosen for the 2 factors (MT, MA). The number of experiments needed was defined by the number of possible combinations of factors and levels (3^2 = 9), and all experiments were performed in triplicate to obtain statistically robust data, leading to a total of 27 experiments. The order of each series of 9 experiments was randomized, to avoid any possible effect due to running sequence.

Data were collected from NOVA 2.1.6 software and elaborated Microsoft Office and Origin 9 Pro software.

2.6. Manufacture of the sensor

15 μL of MWCNT-S-Au dispersion (1 mg mL^{-1}) in Milli-Q water was drop-casted onto the SPCE surface. Then, 70 μL of a 1.15 mmol L^{-1} solution of pyrrole, in the presence of 5-HT (200 mmol L^{-1}), were deposited onto the resulting SPCE/MWCNT-S-Au. MIP-modified SPCE/MWCNT-S-Au was obtained by performing 5 cycles of CV (0 V to +1.00 V, 100 mV s^{-1}) using 0.1 M PBS enriched with 0.1 mol L^{-1} of KCl (pH = 7) as an electrolyte. Subsequently, the embedded 5-HT was eliminated by scanning between - 0.6 and + 1.00 V in 0.1 mol L^{-1} phosphate buffer solution (pH = 7.4) for several cycles until no oxidation peak for 5-HT was observed. As a control, a non-molecularly

imprinted polymer (NIP) modified SPCE/MWCNT-S-Au (SPCE/MWCNT-S-Au/NIP) was also prepared and treated in the same way, except for the omission of 5-HT in the electro-polymerization process. The morphological structures of the modified electrodes were studied by SEM.

2.7. Detection of serotonin and evaluation of sensing performances

The dose-dependent responses of SPCE/MWCNT-S-Au and SPCE/MWCNT-S-Au/MIP were evaluated. In the optimized conditions obtained from the DoE, analyzing 11 solutions spiked with different concentrations of 5-HT (0.5, 1, 2.5, 5, 7.5, 12, 16, 20, 25, 40, 50 μmol L^{-1}). 0.1 mol L^{-1} of PBS enriched with 0.1 mol L^{-1} of KCl (pH = 7) was used as a supporting electrolyte. For SPCE/MWCNT-S-Au/MIP, a potential of −300 mV was applied for 10 s before each measurement to favor the accumulation of the analyte in the MIP.

Sensitivity was calculated as the ratio between the slope of the calibration curve (μA μmol^{-1} L) and the geometric surface area of the Dropsens electrode (~0.126 cm^2). The LOD was determined as 3 times the standard error from the linear regression on the calibration curve divided by the slope of the calibration curve ($\frac{3\sigma}{S}$). Reusability was determined by recording 3 consecutive calibration curves with the same sensor and calculating the percentage standard deviation among the obtained slopes. Reproducibility was determined by recording 3 independent calibration curves with 3 different sensors and by calculating the percentage standard deviation among the obtained slopes.

To evaluate the influence of interfering agents, in the first instance solutions of DA, tryptophan (TRP), uric acid (UA), and ascorbic acid (AA), at the concentrations of 50 mmol L^{-1} in PBS/KCl 0.1 mol L^{-1}, were prepared and DPV measured, in a potential window comprised between −0.2 and 0.5 V. Furthermore, DPV at a constant concentration of interferent (5 μmol L^{-1}) in the presence of varying concentrations of 5-HT (2.5, 5, 7.5, 10, 12.5 μmol L^{-1}) were registered. The slope and intercept of the calibration lines obtained were compared to evaluate the effect of the possible interferents.

3. Results and discussion

3.1. Functionalization of the MWCNTs

In the first instance, we functionalized MWCNTs with thiol groups to later exploit them as anchoring moieties for a stable grafting of Au NPs on the surface of MWCNTs (Fig. 1). To perform this task, we aimed at a two-step, controlled functionalization of the surface, ensuring the protection of the thiols during the functionalization, to make them available for interaction with the Au NPs at the end of the process. Moreover, to facilitate electron transduction from the catalytic site to the conductive material, we aimed to control the length of the linkers on the surface of MWCNTs. Considering all these requirements, we synthesized a disulfide-bearing diazonium salt and used it to perform a radical reaction on the surface of MWCNTs [43,44]. Compared with other approaches, diazonium salts are highly reactive, inducing a high degree of functionalization. However, for this very same reason, their radical reaction is poorly controllable, as it leads to the formation of oligomeric chains that can passivate the material surface, hindering electron transduction. The strategy herein presented allowed us to achieve control over the undesired oligomerization, by cleaving of disulfide bond during the second step of the synthesis (Fig. 1). Indeed, by reducing the disulfide bond, we simultaneously eliminated the oligomeric chains formed during the radical reaction and deprotected the thiol moieties, making them available for anchoring Au NPs [45]. The aryl diazonium salt was synthesized starting from 4-ATP [41], and isolated as a tetrafluoroborate salt, instead of being generated *in situ*, to properly

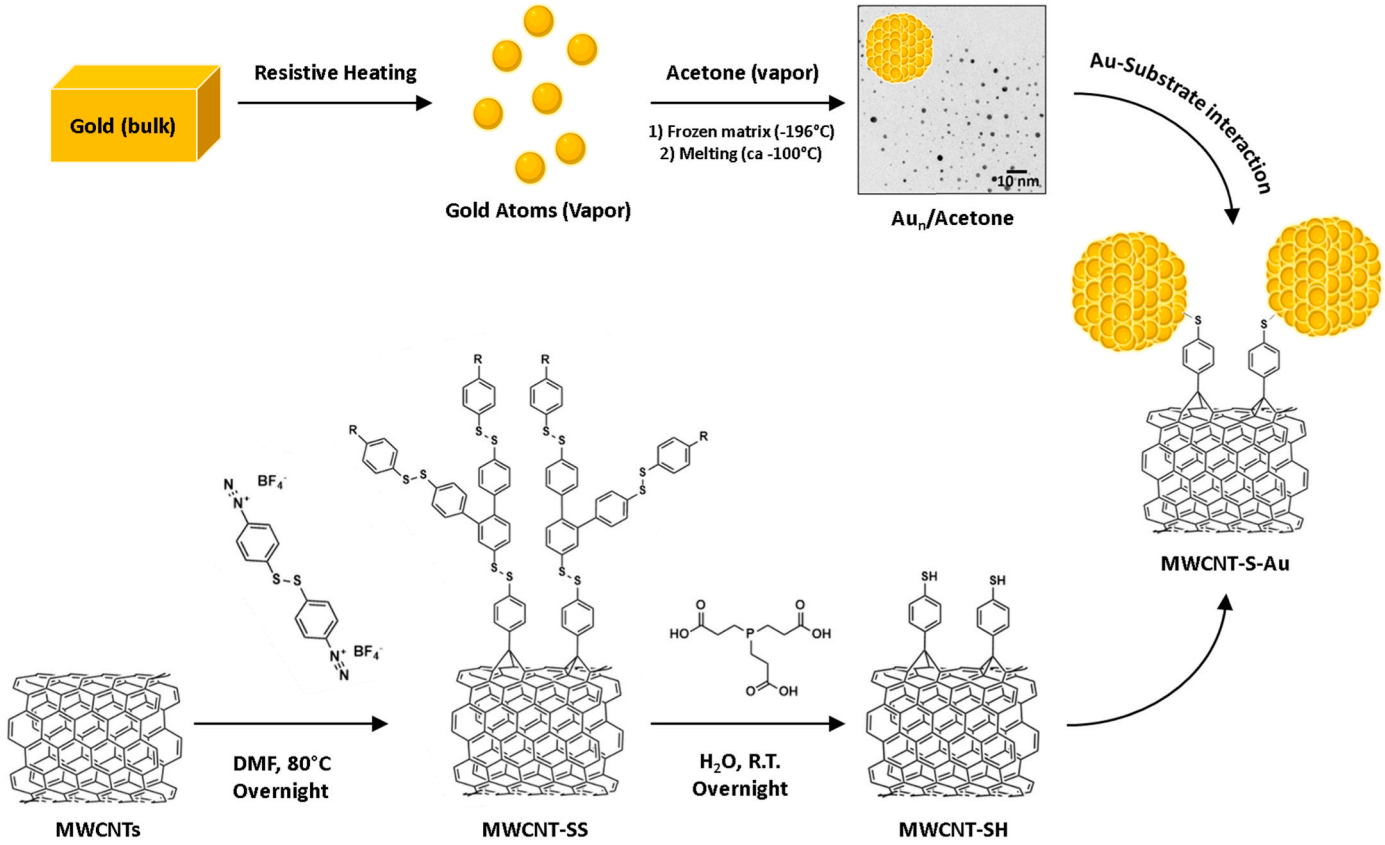

Fig. 1. Synthetic scheme of MWCNT-S-Au, illustrating the functionalization strategy based on a radical reaction and disulfide cleavage to obtain MWCNT-SH and the synthesis of Au NPs by MVS approach and their grafting on MWCNT-SH.

characterize it by ^{1}H NMR and ATR-FTIR (Figs. S1–3) and verify its thermal stability by DSC (Fig. S3). The MWCNT functionalization was performed in DMF to increase the dispersibility of the nanomaterial, and thus the surface area available for functionalization [46].

We characterized all the steps of the functionalization by XPS and TGA (Figs. S4–S7). After the first step of the synthesis, the XPS survey spectrum highlighted an increase in the overall content of Sulfur from an undetectable amount to represent 3.81 % of the atoms composing the material (Table S1). This increase can be imputed to the grafting of the aryl radical on the MWCNT surface [47]. Furthermore, by observing the high-resolution spectrum of the 2p orbitals of Sulfur (Fig. S5a), we can assess that the majority of the sulfur atoms (3,05 %) are involved in S–S/S–H bonds. Disulfides and thiols can be hardly distinguished at XPS as they both fall at a binding energy of around 164 eV. The successful functionalization is also confirmed by the weight loss observed at TGA at 500 °C (Fig. S5c), a temperature at which the organic functionalization is completely degraded, while the graphitic structure of the carbon material is still preserved [48,49]. At this temperature, MWCNT-SS presented a mass loss of 5.77 % that, compared with the mass loss for pristine MWCNTs, allowed us to estimate a degree of functionalization of 119 μmol mg^{-1} of MWCNTs. After the second step of the functionalization, the cleavage of disulfide bonds induced a reduction of the total sulfur atomic percentage to 2.5 %, of which 2 % was related to the SS/SH component (Fig. S5b). The decrease of the sulfur atomic percentage from MWCNT-SS to MWCNT-SH agrees with the cleavage of oligomeric excess on the surface of MWCNTs. Comparing these results with similar synthetic strategies previously reported [45], we can affirm that isolating the diazonium salt and performing the reaction in DMF allowed better control over the functionalization. Indeed, although our TGA measurements show a lower weight loss compared to previous reports [45], XPS highlights that the sulfur atomic percentage in our materials is 5 times higher. This means that we have been able to reduce drastically the amount of excess polymer that is formed during the radical reaction, and consequently, less material is removed during the cleavage, improving the overall mass balance of the process.

3.2. Synthesis and characterization of MWCNT-S-Au

To enhance the innate electrocatalytic properties of MWCNTs toward the oxidation of 5-HT, we modified MWCNTs with Au NPs obtained by the MVS approach (Fig. 1). The well-known catalytic properties of these nanoparticles, imparted by their small dimension and weakly coordinated metallic surface [35–38], were herein exploited for the first time in the design of an electrochemical sensor. Using the MVS reactor, Au atoms, produced by resistive heating of the metal under high vacuum, were co-condensed at liquid nitrogen temperature (−196 °C) with acetone vapors. On warming until the solid matrix melted (ca. −95 °C), a deep-purple solution containing small Au NPs (2–4 nm) stabilized by the excess of the organic solvents acting as weakly coordinating ligands, was obtained. It was exploited as a source of pre-formed ligand-free Au NPs. Therefore, Au NPs were immobilized on MWCNT-SH by simple impregnation at 25 °C, removing their excess and washing accurately the resulting material (Fig. 1).

The final amount of immobilized Au grafted on the MWCNTs was determined to be 11.55 % by ICP-MS and 12.4 % by TGA (Fig. 2a). AuNP oxidation state was investigated by XPS (Fig. 2b). The main component of the Au 4f$_{7/2}$ core was centered at the binding energy of 84.08 eV, which is in agreement with an oxidation state of Au^{0} [50,51]. This component, which represents 96.3 % of the total Au, demonstrates that the majority of gold atoms composing the NPs are metallic, comprised

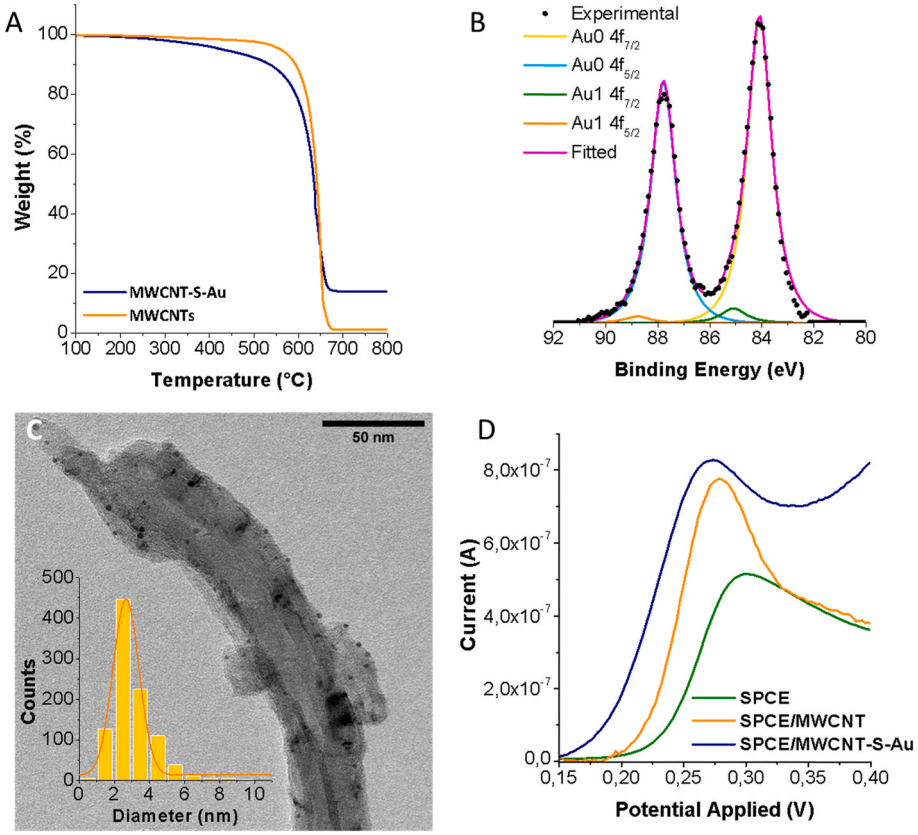

Fig. 2. Characterization of MWCNT-S-Au. A) TGA of MWCNTs and MWCNT-S-Au in the air; B) High-resolution XPS spectrum of Au4f orbitals of MWCNT-S-Au; C) TEM micrograph of MWCNT-S-Au with size distribution analysis of Au NPs on the surface of the material; D) LSV voltammograms for 12 μmol L^{-1}solutions of 5-HT on bare and modified SPCEs. The voltammograms were recorded by scanning applied potential from 0.1 to 0.4 V, with a scan rate of 20 mV s^{-1}, and were baseline-subtracted.

those on the surface, in agreement with previously reported MVS Au NPs deposited onto different supports [36,37,52].

By TEM (Fig. 2c, Fig. S8) we examined the topology of the MWCNT-S-Au and it revealed the presence of spherical Au NPs having an average diameter of 2.9 ± 1.2 nm, optimal for electrocatalytic applications [53,54], that were highly dispersed on the surface of the nanotubes without the presence of Au NPs agglomerates. The presence of gold in the nanocomposite was assessed also by CV, comparing the voltammetric response of MWCNT-S-Au with MWCNT-SH using 0.1 M PBS +0.1 M KCl as a supporting electrolyte. We observed the appearance of a peak related to the oxidation of Au^0 to Au^+ at 0.9 V, a potential comparable to data previously reported in the literature for Au NPs (Fig. S9) [55,56].

Finally, we assessed the electrocatalytic activity of MWCNT-S-Au for serotonin oxidation by LSV. We compared the performance of a non-modified SPCE, with SPCEs modified with MWCNTs and MWCNT-S-Au (Fig. 2d) [57]. As expected, both modifications induced an anticipation of the oxidation peak and an increase of the faradaic current. However, the grafting of Au NPs allows us to further anticipate the onset potential of the reaction of 50 mV. This means that MWCNT-S-Au effectively reduces the onset potential and improves the rate of the reaction.

3.3. Evaluation of sensing performances of SPCE/MWCNT-S-Au

To evaluate the applicability of our composite material in 5-HT sensing and its dose-dependent response, we selected DPV as an analytical technique. This technique is designed to minimize the contribution of background capacitive current [58,59], improving the sensitivity and signal-to-noise ratio of the final sensor [58].

This electrochemical technique is particularly useful in the case of modified nanostructured electrodes, where carbon nanomaterials and conductive polymers induce an increase of capacitive current (Fig. S10) that limits the performances in terms of LOD [60]. In DPV, the optimization of the operational parameters is a complicated and crucial step that dramatically affects the final performance of the analysis. To identify the best operational parameters, we modified SPCE with MWCNT-S-Au (SPCE/MWCNT-S-Au), and we applied a DoE [61], focusing on the two main parameters that influence the performances of DPV: the modulation amplitude, which is the intensity of each potential pulse, and the modulation time which is the duration of the pulses [42]. We used a factorial design, choosing three equally spaced levels for each of the two parameters, and we formulated all the possible combinations of factors and levels (n = 9). We then performed the experiments in triplicate using the same electrode (SPCE/MWCNT-S-Au) and the sequence of experiments was randomized for each series. Within this DoE we aimed to maximize the peak resolution, the current intensity, and the signal-to-noise ratio. A first figure of merit (FoM1) has been identified to describe intense and sharp peaks, which can be obtained when the ratio between the faradaic current (i_F) and the width of the peak at medium height ($\Delta E_{1/2}$) is maximized as described in **Equation (1)**.

$$FoM1 = \frac{i_F}{\Delta E_{1/2}} \quad \text{Eq. 1}$$

Therefore, this FoM1 will be used to identify the conditions to optimize the sensitivity and resolution of the voltammetric analysis.

On the other hand, a high signal-to-noise ratio can be achieved when the ratio between the faradaic current (i_F) and the baseline current sampled immediately before the start of the oxidation peak (i_b) is maximized as described in FoM2 (**Equation (2)**).

$$FoM2 = \frac{i_F}{i_b} \quad \text{Eq. 2}$$

The maximization of FoM2 will allow us to obtain a sensor with a low LOD.

From the three series of experiments performed, we determined the average value of both the two previously described FoMs (Figure S11 a, b) and applied a multiple regression, to obtain the final 3D functions (Figure S12 a, b) which describe the variation of these FoMs in the function of MT and MA. More information regarding the DoE and the respective results are reported in SI. From the DoE, it results that the maximization of FoM1 requires low MT and high MA (Fig. S12a). However, these conditions do not allow an efficient decay of the background capacitive current i_b, thus leading to a low signal-to-noise ratio and affecting the LOD. On the other hand, the maximization of FoM2 was achieved for high MT and low MA (Fig. S12b), conditions in which low peak currents are registered. As a result, the maximization of FoM1 and FoM2 offers opposite solution, meaning that to optimize one means to sacrifice the other. Therefore, aiming to achieve a good compromise between high sensitivity, good resolution, and low limits of detection, we defined a third FoM (**Equation (3)**), which is the product of the two previous normalized functions.

$$FoM3 = \frac{i_F^2}{\Delta E_{1/2} i_b} \quad \text{Eq. 3}$$

From this final function, we determined the average values for each selected level (Fig. S13) and obtained the surface of response represented in Fig. 3a. From this surface of response, we interpolated the optimal values of MT (0.01 s) and MA (0.075 V), which were subsequently used for all the following sensing experiments. We tested the optimized conditions for sensing with SPCE/MWCNT-S-Au by performing DPV of eleven solutions of serotonin at different concentrations (from 0.5 to 50 μmol L^{-1}, Fig. 3b and **c**). The response of the modified electrode was linear in the range of 1–12 μmol L^{-1} (Fig. 3d), with a R^2 = 0.98934, sensitivity of 17.4 μA μmol^{-1} L^{-1} cm^{-2} and a LOD of 1.9 μmol L^{-1}.

For SPCE/MWCNT-S-Au, we determined a reusability standard deviation of 20.8 % and a reproducibility standard deviation of 9.5 % (Fig. S14). The high standard deviation for the reusability could be.

Associated with adsorption phenomena and consequent passivation of the surface of the electroactive material in consecutive analysis.

Finally, we studied the influence of common interfering agents for 5-HT sensing (AA, DA, TRP, and UA), by performing DPV of 50 μmol L^{-1} solutions of each species in PBS/KCl 0.1 mol L^{-1} over a scan range from −0.20 to 0.50 V. As shown in Fig. 3e, no response could be detected for both AA and TRP in the observed potential range, while an intense peak for DA is present at 0.10 V. In the conditions optimized through the DoE, the peaks of DA and 5-HT are resolved enough not only to neglect any mutual interference but also to allow the simultaneous detection of the two neurotransmitters, broadening the applicability of the electroactive material for sensing purposes. The only specie oxidized at the same potential of 5-HT is UA, with a ΔE between the two oxidation peaks of only 23 mV. However, the sensitivity for UA is significantly lower, as the current generated by the oxidation of UA is 8.8 times lower compared to the current generated by serotonin oxidation. Four calibration lines for 5-HT were registered in the linear range, each one with a constant concentration (5 μmol L^{-1}) of one of the possible interferent. Comparing the slopes and the intercepts of the calibration lines, we can confirm that UA is the only interferent for this system (Fig. S15).

3.4. Electro-polymerization of the MIP

Aiming at enhancing the selectivity of the sensor for 5-HT, as well as at providing antifouling properties to its surface, we used electro-polymerized molecularly imprinted polypyrrole to further modify the surface of the sensor. MIPs are synthetic receptors prepared by polymerization of monomers, crosslinkers, and other essential constituents in the presence of the target analyte as a template [62]. This process leads to a highly cross-linked three-dimensional polymer network [63]. We chose to prepare MIP by electro-polymerization, as it offers precise

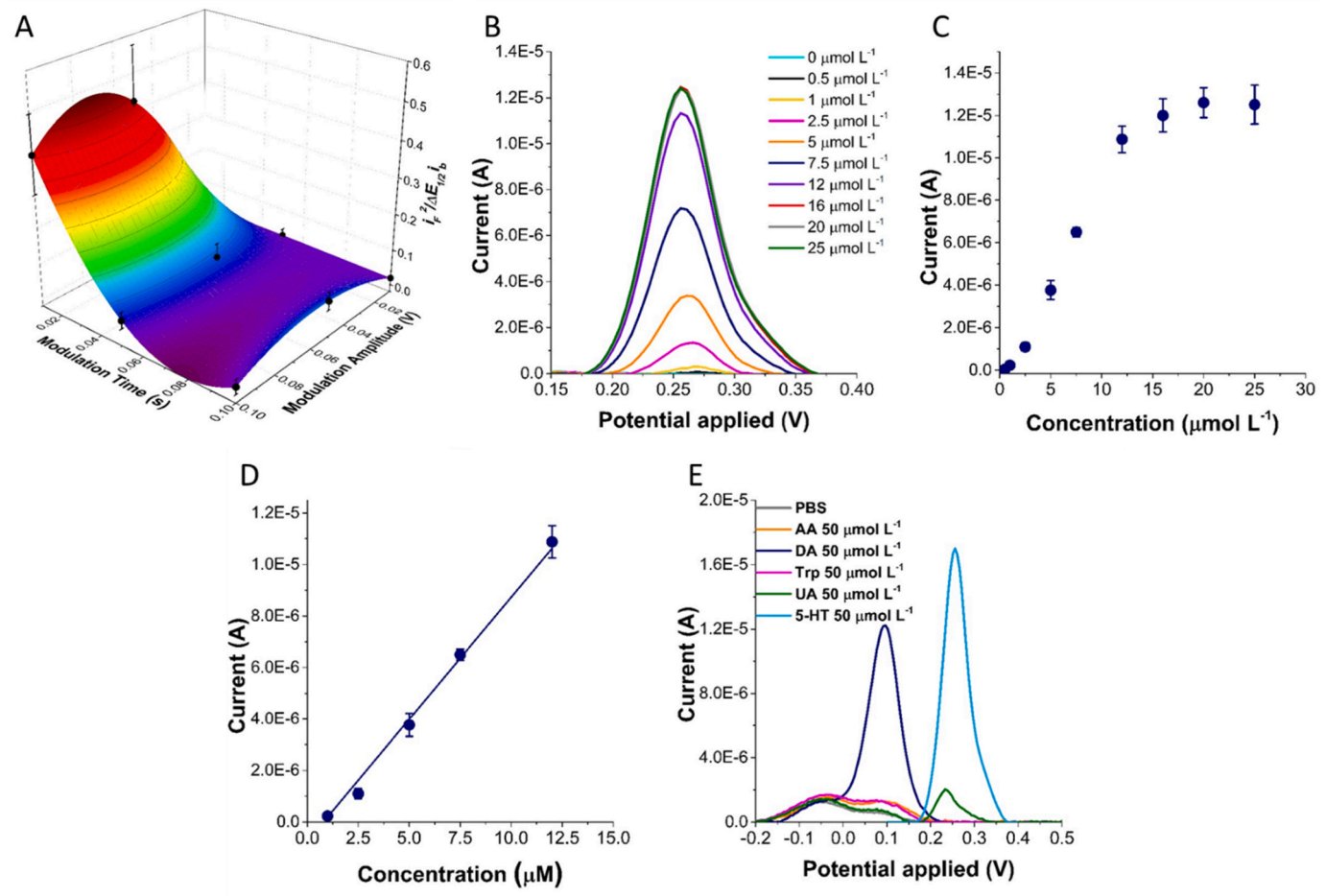

Fig. 3. A) FoM3 derived from DoE; B) DPV response of SPCE/MWCNT-S-Au to 0.5, 1.0, 2.5, 5.0, 7.5, 12.0, 16.0, 20.0, 25.0 µmol L^{-1} solutions of 5-HT in optimized conditions (MT = 0.01 s; MA = 0.075 V, IT = 0.250 s; step potential = 0.005 V).; C) Calibration curve in the range from 0.5 to 25.0 µmol L^{-1}; D) Linear regression in the range from 2.5 to 12.0 µmol L^{-1}; E) DPV of different interfering agents (AA, DA, Trp, UA) at the concentration of 50 mmol L^{-1} in PBS buffer (MT = 0.01 s; MA = 0.075 V, IT = 0.250 s; step potential = 0.005 V).

control over polymer morphology and site-specific functionalization, enhancing MIP selectivity and recognition capabilities. It also enables fast polymerization kinetics and efficient template removal steps, simplifying the synthesis process while maintaining high reproducibility and offering environmental benefits through reduced use of hazardous chemicals. A scheme resuming the synthesis of the MIP is reported in Fig. 4a. After functionalization of the SPCE, the obtained SPCE/MWCNT-S-Au was incubated with a solution of pyrrole in the presence of a large excess of 5-HT. Electro-polymerization was carried out *in situ* performing 5 consecutive cyclic voltammetry. After the removal of 5-HT by means of electrochemical overoxidation, the final sensor (SPCE/MWCNT-S-Au/MIP) is obtained. Further details about MIP electro-polymerization and characterization can be found in SI (Figs. S16–S19).

We characterized the surface of the modified SPCEs by scanning electron microscopy (SEM). In Fig. 4b it is possible to observe how MWCNT-S-Au are distributed across the SPCE surface, creating a 3D network structure, which significantly improves the electrode area of the SPCE. It is worth noting that the thickness of the MIP layer in electrochemical sensors is of high importance since it directly impacts the electron transfer efficiency, sensitivity, diffusion kinetics, mechanical stability, and reproducibility of the biosensor [64]. Thus, fine control of this parameter is essential for achieving high-performance electrochemical sensors with reliable and accurate detection capabilities. Indeed, different concentrations of pyrrole were tested. The use of concentrations higher than 1.15 mmol L^{-1} led to the over-growth of the polymer on the surface of the electrode (Fig. S17), causing higher passivation and negatively influencing the performance of the sensor.

After electro-polymerization, the morphology of the MWCNTs 3D network is retained (Fig. 4c), with an increase in the average diameter of MWCNT-S-Au from 30 ± 8 nm to 45 ± 10 nm for MWCNT-S-Au/MIP (Fig. 4d). Therefore, it can be concluded that the MIP has been deposited as a controlled film of 7.5 nm covering the 3D network. In addition, a lower electron detector (LED) was used instead of the upper secondary electron detector (USD) to prove that the AuNPs were not affected after the polymerization (Fig. S18). Brighter spheres can be observed, confirming the presence of the metallic particles below the MIP layer.

As a control (SPCE/MWCNT-S-Au/NIP), a non-molecularly imprinted polymer (NIP) was created to modify the SPCE/MWCNT-S-Au, using the same process previously described, in the absence of serotonin during the electro-polymerization step. SEM analysis highlighted that no differences can be observed between MWCNT-Au-NIP/SPCE (Fig. S19) and MWCNT-Au-MIP/SPCE (Fig. 4c). As shown in Fig. 4e, the difference in the electrochemical response of the two modified electrodes demonstrates the efficiency of the molecular imprinting.

3.5. Evaluation of the sensing performances of SPCE/MWCNT-S-Au/MIP

Finally, we evaluated the performance of the final sensor toward the detection of 5-HT. In the first instance, we studied the response of SPCE/MWCNT-S-Au/MIP in PBS, by performing DPV measurements of 8 solutions of 5-HT (from 1 µmol L^{-1} to 25 µmol L^{-1}), using the conditions

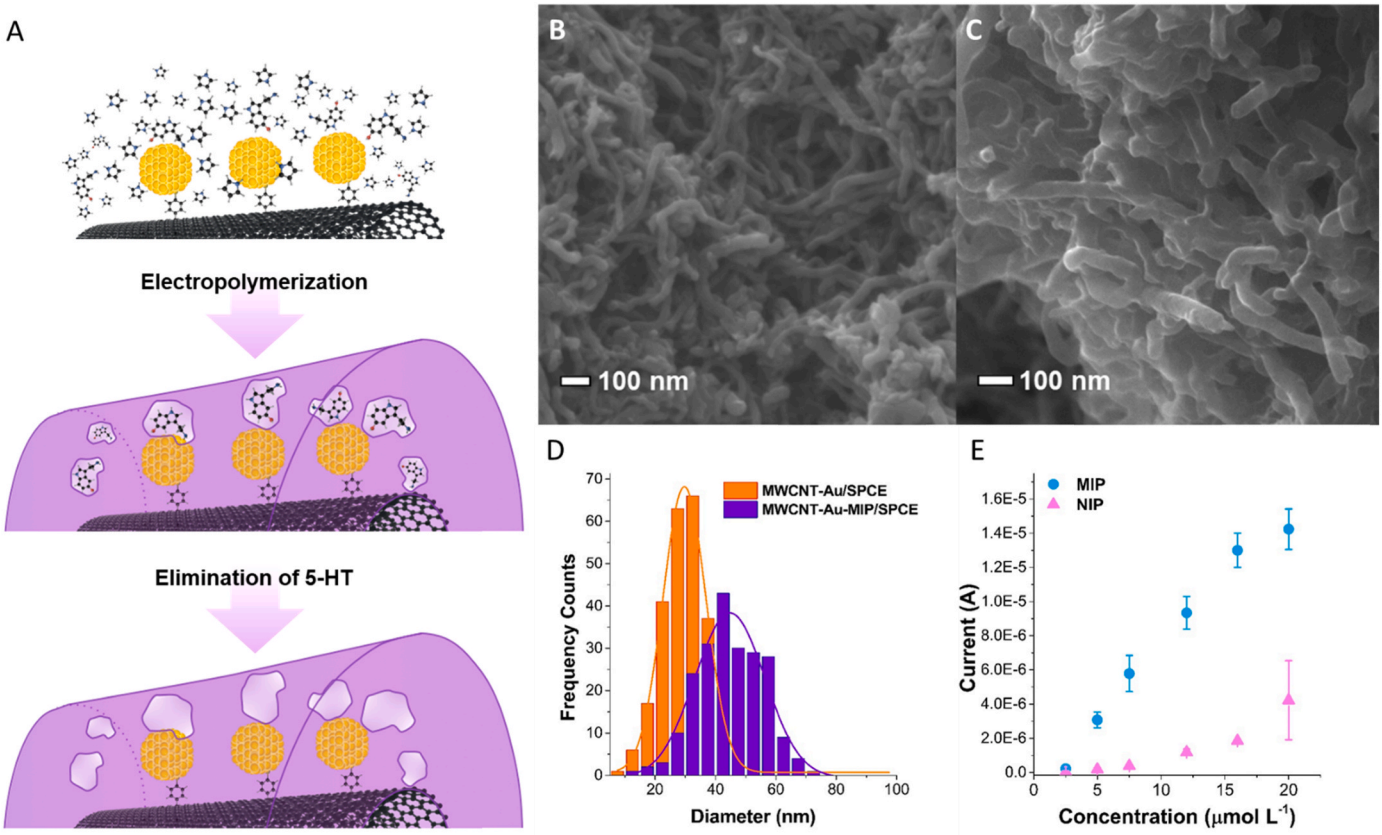

Fig. 4. Electro-polymerization of 5-HT selective MIP A) Schematic representation of The MIP polymerization of MIP on the surface of SPCE/MWCNT-S-Au; B) SEM image of the working electrode of SPCE/MWCNT-S-Au; C) SEM image of the working electrode SPCE/MWCNT-S-Au/MIP; D) Statistical dimensional analysis of the diameter of MWCNTs in the modified SPCE; E) DPV response of SPCE/MWCNT-S-Au/MIP and SPCE/MWCNT-S-Au/NIP to 2.5, 5.0, 7.5, 12.0, 16.0, 20.0 μmol L^{-1} solutions of 5-HT. DP voltammograms were recorded with the parameters optimized with the DoE (MT = 0.01 s; MA = 0.075 V, IT = 0.250 s; step potential = 0.005 V).

optimized for SPCE/MWCNT-S-Au. After the polymerization of the MIP on the surface of the sensor, we observed a decrease in the sensitivity and LOD higher if compared to SPCE/MWCNT-S-Au. As well a change in the linear range was observed, which for SPCE/MWCNT-S-Au/MIP was comprised between 7.5 and 25 μmol L^{-1}. The worsening of the performance could be related to the presence of the MIP that hinders the electroactive material and slows down the diffusion of 5-HT through the polymeric network toward the catalytic sites. Therefore, to enhance sensitivity, we applied adsorptive stripping to pre-accumulated 5-HT on the surface of the working electrode [65], fully exploiting two properties of the MIP, specifically its high capacitance and the selective supramolecular interactions with 5-HT.

Since 5-HT is positively charged at neutral pH, we studied the application of negative potentials to favor the migration of 5-HT molecules toward the functionalized surface. We found out that applying a potential of −300 mV for 10 s before each measurement can sensitively increase the response of the sensor for 5-HT (Fig. 5). The use of negative polarization can provide a second benefit: to repel the negatively

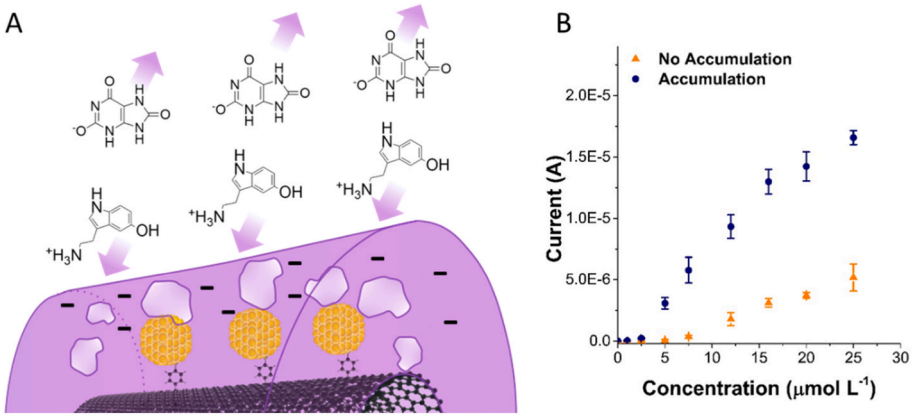

Fig. 5. A) Pre-accumulation of 5-HT on the surface of the electrode; B) calibration curves for 5-HT with SPCE/MWCNT-S-Au/MIP with and without adsorptive stripping. Calibration curves were obtained from DPV measurements recorded with the parameters optimized with the DoE (MT = 0.01 s; MA = 0.075 V, IT = 0.250 s; step potential = 0.005 V).

charged UA, which in the previous section was identified as the major interferent of this system.

In the final conditions, applying the pre-accumulation potential, the sensor shows a wider linear range from 2.5 to 20 μmol L^{-1}, with good linearity ($R^2 = 0.99901$), sensitivity of 8.0 μA μmol^{-1} L cm^{-2} and a LOD of 1.7 μ mol L^{-1} (Fig. 6a–b). Moreover, the presence of MIP reusability and reproducibility with a relative SD of 4.4 % and 1.1 % respectively solved the problems of absorption highlighted with SPCE/MWCNT-S-Au. This level of reproducibility is higher than many other sensors previously reported (Table S7).

To investigate why for concentrations higher than 20 μmol L^{-1} a limit current and plateaux are reached, we performed CVs at different scan rates and studied the correlation between the increase in current and the scan rate (Fig. S20). The analysis highlights that the peak current increases linearly with the scan.

Rate, identifying that 5-HT oxidation is an adsorption-limited process. Therefore, we can conclude that at concentrations higher than 20 μmol L^{-1} a saturation of the catalytic sites of the electroactive material takes place due to 5-HT absorption.

Then, we demonstrated that the sensor could function in a more complex matrix by performing the detection of 5-HT in spiked solutions of fetal bovine serum (FBS). FBS is a challenging testbed for the proposed sensor as it contains over 1000 different components, including lipids, growth factors, hormones, and proteins. In the absence of the MIP, when the surface of the electrocatalytic material is exposed to the complex matrix, non-specific irreversible adsorption of biomolecules takes place, fouling the surface of the electrode and inducing a severe shift of oxidation potential (Fig. 6c). Indeed, in these conditions, SPCE/MWCNT-S-Au shows no linear response at increasing concentrations of 5-HT.

On the other hand, the response of the SPCE/MWCNT-S-Au/MIP is preserved in FBS, with no significant shift in the oxidation peak potential (Fig. 6d), and a linear in the range comprised between 1 up to 12 μmol L^{-1} (Fig. 6e), with $R^2 = 0.9922$. The sensitivity (6.7 μA μ mol^{-1} L cm^{-2}) and LOD (1.0 μmol L^{-1}) are comparable to those registered in PBS. Furthermore, SPCE/MWCNT-S-Au/MIP showed optimal reusability and reproducibility (Fig. S21). The anodic current registered in the absence of spiked 5-HT can be explained by the presence of native 5-HT and possible interference due to the high levels of uric acid present in FBS. In conclusion, the MIP not only provides the electrode with selectivity for 5-HT but also prevents fouling, allowing it to operate in complex biological fluids rich in bio-macromolecules.

4. Conclusions

Herein we presented a robust and reliable voltammetric sensor for the detection of 5-HT in plasma. The sensor was meticulously designed from the synthesis of the electrocatalytic transducer to the optimization of the analytical parameters. MWCNTs decorated with small and highly active Au NPs were obtained by applying a functionalization strategy that allowed us to protect the SH moieties during the radical reaction while controlling the distance between the MWCNTs and the Au NPs. This fine control allowed us to favor the electron transfer between the two materials, improving the sensitivity of the final sensor. Selectivity and antifouling properties were conferred to the sensor using a thin layer (7.5 nm) of 5-HT selective MIP. Furthermore, we exploited the high capacitance of PPy to accumulate 5-HT in the MIP cavities by negatively polarizing the electrode. Another innovative aspect of the work is represented by the application of DoE optimizing the analytical performances of DPV-based sensors (e.g. sensitivity, LOD, and resolution). This sensor, able to detect 5-HT in few second everywhere and at any moment, has a huge potential in the continues monitoring of serotonin-

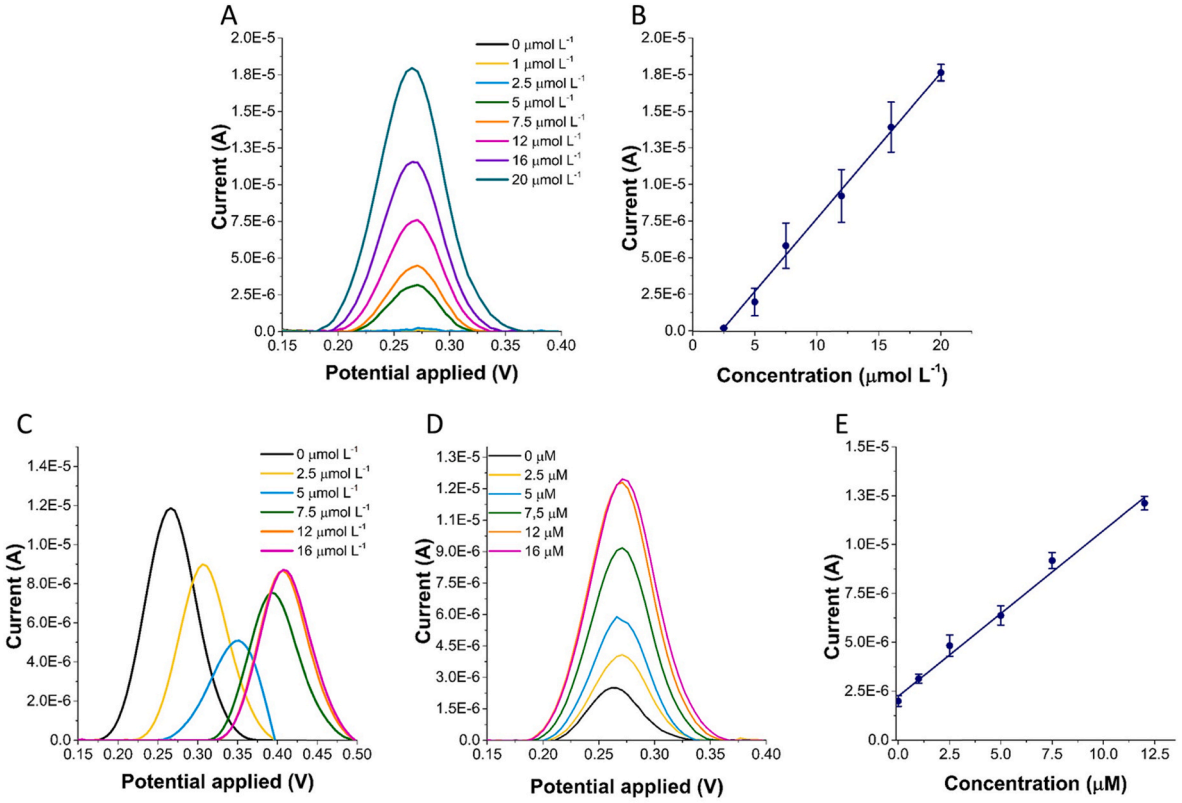

Fig. 6. A) DPV response of SPCE/MWCNT-S-Au/MIP to different concentrations of 5-HT in PBS; B) calibration curve for SPCE/MWCNT-S-Au/MIP in PBS; C) DPV response of SPCE/MWCNT-S-Au to different solutions of 5-HT in FBS/PBS 1:4; D) DPV response of SPCE/MWCNT-S-Au/MIP to different concentrations of 5-HT in FBS/PBS 1:4; E) calibration curve for SPCE/MWCNT-S-Au/MIP in FBS/PBS 1:4. DP voltammograms were recorded with the parameters optimized with the DoE (MT = 0.01 s; MA = 0.075 V, IT = 0.250 s; step potential = 0.005 V).

related diseases, especially for those requiring a timely diagnosis, such as serotonin fatal syndrome.

CRediT authorship contribution statement

Giuseppe Misia: Writing – review & editing, Writing – original draft, Validation, Methodology, Investigation, Formal analysis, Data curation, Conceptualization. **Claudio Evangelisti:** Writing – review & editing, Supervision, Methodology, Investigation, Conceptualization. **Juan P. Merino:** Writing – review & editing, Methodology, Investigation. **Emanuela Pitzalis:** Writing – review & editing, Methodology, Investigation. **Adrián M. Abelairas:** Writing – review & editing, Methodology, Investigation. **Jesús Mosquera:** Writing – review & editing, Funding acquisition. **Alejandro Criado:** Writing – review & editing, Supervision, Methodology, Investigation, Funding acquisition, Formal analysis, Conceptualization. **Maurizio Prato:** Writing – review & editing, Supervision, Funding acquisition. **Alessandro Silvestri:** Writing – review & editing, Writing – original draft, Supervision, Methodology, Investigation, Formal analysis, Data curation, Conceptualization.

Declaration of competing interest

The authors declare the following financial interests/personal relationships which may be considered as potential competing interests: Alejandro Criado reports financial support was provided by Spain Ministry of Science and Innovation. Jesus Mosquera reports financial support was provided by Spain Ministry of Science and Innovation. If there are other authors, they declare that they have no known competing financial interests or personal relationships that could have appeared to influence the work reported in this paper.

Acknowledgments

A.C. and J.M. acknowledge financial support by MCIN/AEI/10.13039/501100011033 and "ESF: Investing in Your Future" (Grant RYC2020-030183-I to A.C., RYC2019-027842-I to J.M., PID2021-127002NA-I00 to A.C., PID2020-117885 GA-I00 to J.M.).

Appendix A. Supplementary data

Supplementary data to this article can be found online at https://doi.org/10.1016/j.carbon.2024.119550.

References

[1] C. Jonnakuty, C. Gragnoli, What do we know about serotonin? J. Cell. Physiol. 217 (2008) 301–306, https://doi.org/10.1002/jcp.21533.
[2] L.A. Jones, E.W. Sun, A.M. Martin, D.J. Keating, The ever-changing roles of serotonin, Int. J. Biochem. Cell Biol. 125 (2020) 105776, https://doi.org/10.1016/j.biocel.2020.105776.
[3] M. Pourhamzeh, F.G. Moravej, M. Arabi, E. Shahriari, S. Mehrabi, R. Ward, R. Ahadi, M.T. Joghataei, The roles of serotonin in neuropsychiatric disorders, Cell. Mol. Neurobiol. 42 (2022) 1671–1692, https://doi.org/10.1007/s10571-021-01064-9.
[4] A. Colao, C. Pivonello, Serotonin, in: S. La Rosa, S. Uccella (Eds.), Endocr Pathol, Springer International Publishing, Cham, 2022, pp. 730–731, https://doi.org/10.1007/978-3-030-62345-6_5120.
[5] C. Pagan, R. Delorme, J. Callebert, H. Goubran-Botros, F. Amsellem, X. Drouot, C. Boudebesse, K. Le Dudal, N. Ngo-Nguyen, H. Laouamri, C. Gillberg, M. Leboyer, T. Bourgeron, J.-M. Launay, The serotonin-N-acetylserotonin–melatonin pathway as a biomarker for autism spectrum disorders, Transl. Psychiatry 4 (2014) e479, https://doi.org/10.1038/tp.2014.120, e479.
[6] G. Fanciulli, R.M. Ruggeri, E. Grossrubatscher, F. Lo Calzo, T.D. Wood, A. Faggiano, A. Isidori, A. Colao, On behalf of NIKE, Serotonin pathway in carcinoid syndrome: clinical, diagnostic, prognostic and therapeutic implications, Rev. Endocr. Metab. Disord. 21 (2020) 599–612, https://doi.org/10.1007/s11154-020-09547-8.
[7] M. Rieder, N. Gauchel, C. Bode, D. Duerschmied, Serotonin: a platelet hormone modulating cardiovascular disease, J. Thromb. Thrombolysis 52 (2021) 42–47, https://doi.org/10.1007/s11239-020-02331-0.
[8] B. Spivak, Y. Vered, R. Yoran-Hegesh, E. Averbuch, R. Mester, E. Graf, A. Weizman, Circulatory levels of catecholamines, serotonin and lipids in attention deficit hyperactivity diiorder, Acta Psychiatr. Scand. 99 (1999) 300–304, https://doi.org/10.1111/j.1600-0447.1999.tb07229.x.
[9] M. Moriarty, A. Lee, B. O'Connell, A. Kelleher, H. Keeley, A. Furey, Development of an LC-MS/MS method for the analysis of serotonin and related compounds in urine and the identification of a potential biomarker for attention deficit hyperactivity/hyperkinetic disorder, Anal. Bioanal. Chem. 401 (2011) 2481–2493, https://doi.org/10.1007/s00216-011-5322-7.
[10] K. Hara, Y. Hirowatari, Y. Shimura, H. Takahashi, Serotonin levels in platelet-poor plasma and whole blood in people with type 2 diabetes with chronic kidney disease, Diabetes Res. Clin. Pract. 94 (2011) 167–171, https://doi.org/10.1016/j.diabres.2011.06.020.
[11] J. Moncrieff, R.E. Cooper, T. Stockmann, S. Amendola, M.P. Hengartner, M. A. Horowitz, The serotonin theory of depression: a systematic umbrella review of the evidence, Mol. Psychiatr. 28 (2023) 3243–3256, https://doi.org/10.1038/s41380-022-01661-0.
[12] S. Jauhar, D. Arnone, D.S. Baldwin, M. Bloomfield, M. Browning, A.J. Cleare, P. Corlett, J.F.W. Deakin, D. Erritzoe, C. Fu, P. Fusar-Poli, G.M. Goodwin, J. Hayes, R. Howard, O.D. Howes, M.F. Juruena, R.W. Lam, S.M. Lawrie, H. McAllister-Williams, S. Marwaha, D. Matuskey, R.A. McCutcheon, D.J. Nutt, C. Pariante, T. Pillinger, R. Radhakrishnan, J. Rucker, S. Selvaraj, P. Stokes, R. Upthegrove, N. Yalin, L. Yatham, A.H. Young, R. Zahn, P.J. Cowen, A leaky umbrella has little value: evidence clearly indicates the serotonin system is implicated in depression, Mol. Psychiatr. 28 (2023) 3149–3152, https://doi.org/10.1038/s41380-023-02095-y.
[13] S. Ha, B. Jin, B. Clemmensen, P. Park, S. Mahboob, V. Gladwill, F.M. Lovely, A. Gottfried-Blackmore, A. Habtezion, S. Verma, S. Ro, Serotonin is elevated in COVID-19-associated diarrhoea, Gut 70 (2021) 2015, https://doi.org/10.1136/gutjnl-2020-323542.
[14] A. Kumar, R.M. Russell, R. Pifer, Z. Menezes-Garcia, S. Cuesta, S. Narayanan, J. B. MacMillan, V. Sperandio, The serotonin neurotransmitter modulates virulence of enteric pathogens, Cell Host Microbe 28 (2020) 41–53.e8, https://doi.org/10.1016/j.chom.2020.05.004.
[15] L. Lin, X. Jiang, Z. Zhang, S. Huang, Z. Zhang, Z. Fang, Z. Gu, L. Gao, H. Shi, L. Mai, Y. Liu, X. Lin, R. Lai, Z. Yan, X. Li, H. Shan, Gastrointestinal symptoms of 95 cases with SARS-CoV-2 infection, Gut 69 (2020) 997, https://doi.org/10.1136/gutjnl-2020-321013.
[16] L.D. Knecht, G. O'Connor, R. Mittal, X.Z. Liu, P. Daftarian, S.K. Deo, S. Daunert, Serotonin activates bacterial quorum sensing and enhances the virulence of Pseudomonas aeruginosa in the host, EBioMedicine 9 (2016) 161–169, https://doi.org/10.1016/j.ebiom.2016.05.037.
[17] G. Di Giovanni, P. De Deurwaerdère, Serotonin research: crossing scales and boundaries, Neuropharmacology 181 (2020) 108340, https://doi.org/10.1016/j.neuropharm.2020.108340.
[18] A. Spadaro, K.R. Scott, A. Koyfman, B. Long, High risk and low prevalence diseases: serotonin syndrome, Am. J. Emerg. Med. 61 (2022) 90–97, https://doi.org/10.1016/j.ajem.2022.08.030.
[19] S. Prakash, C. Rathore, K. Rana, A. Prakash, Fatal serotonin syndrome: a systematic review of 56 cases in the literature, Clin. Toxicol. 59 (2021) 89–100, https://doi.org/10.1080/15563650.2020.1839662.
[20] Q. He, M. Li, X. Wang, Z. Xia, Y. Du, Y. Li, L. Wei, J. Shang, A simple, efficient and rapid HPLC–UV method for the detection of 5-HT in RIN-14B cell extract and cell culture medium, BMC Chem 13 (2019) 76, https://doi.org/10.1186/s13065-019-0591-x.
[21] M. Lindström, N. Tohmola, R. Renkonen, E. Hämäläinen, C. Schalin-Jäntti, O. Itkonen, Comparison of serum serotonin and serum 5-HIAA LC-MS/MS assays in the diagnosis of serotonin producing neuroendocrine neoplasms: a pilot study, Clin. Chim. Acta 482 (2018) 78–83, https://doi.org/10.1016/j.cca.2018.03.030.
[22] L. Ma, T. Zhao, P. Zhang, M. Liu, H. Shi, W. Kang, Determination of monoamine neurotransmitters and metabolites by high-performance liquid chromatography based on Ag(III) complex chemiluminescence detection, Anal. Biochem. 593 (2020) 113594, https://doi.org/10.1016/j.ab.2020.113594.
[23] J.M. Feldman, Urinary serotonin in the diagnosis of carcinoid tumors, Clin. Chem. 32 (1986) 840–844, https://doi.org/10.1093/clinchem/32.5.840.
[24] A.J. Steckl, P. Ray, Stress biomarkers in biological fluids and their point-of-use detection, ACS Sens. 3 (2018) 2025–2044, https://doi.org/10.1021/acssensors.8b00726.
[25] M.S. Karbownik, S.D. Hicks, The association of salivary serotonin with mood and cardio-autonomic function: a preliminary report, Front. Psychiatr. 13 (2022). https://www.frontiersin.org/journals/psychiatry/articles/10.3389/fpsyt.2022.788153.
[26] E. Cuniberto, Z. Huang, M.D. Ward, D. Shahrjerdi, Unraveling the complex electrochemistry of serotonin using engineered graphitic sensors, Analyst 148 (2023) 105–113, https://doi.org/10.1039/D2AN01451C.
[27] N. Nakatsuka, A. Faillétaz, D. Eggemann, C. Forró, J. Vörös, D. Momotenko, Aptamer conformational change enables serotonin biosensing with nanopipettes, Anal. Chem. 93 (2021) 4033–4041, https://doi.org/10.1021/acs.analchem.0c05038.
[28] N. Nakatsuka, K.J. Heard, A. Faillétaz, D. Momotenko, J. Vörös, F.H. Gage, K. C. Vadodaria, Sensing serotonin secreted from human serotonergic neurons using aptamer-modified nanopipettes, Mol. Psychiatr. 26 (2021) 2753–2763, https://doi.org/10.1038/s41380-021-01066-5.
[29] Q.-Q. Xu, L. Luo, Z.-G. Liu, Z. Guo, X.-J. Huang, Highly sensitive and selective serotonin (5-HT) electrochemical sensor based on ultrafine Fe3O4 nanoparticles anchored on carbon spheres, Biosens. Bioelectron. 222 (2023) 114990, https://doi.org/10.1016/j.bios.2022.114990.

[30] A. Yılmaz Kabaca, M. Bilgi Kamaç, M. Yılmaz, T. Atıcı, Ultra-sensitive electrochemical sensors for simultaneous determination of dopamine and serotonin based on titanium oxide-gold nanoparticles-poly Nile blue (in deep eutectic solvent), Electrochim. Acta 467 (2023) 143046, https://doi.org/10.1016/j.electacta.2023.143046.
[31] Y. Liu, M. Li, B. Zhou, X. Xuan, H. Li, B. Flexible, N co-doped graphene electrodes for electrochemical detection of serotonin in bodily fluids, Electrochim. Acta 457 (2023) 142494, https://doi.org/10.1016/j.electacta.2023.142494.
[32] B. Wu, S. Yeasmin, Y. Liu, L.-J. Cheng, Sensitive and selective electrochemical sensor for serotonin detection based on ferrocene-gold nanoparticles decorated multiwall carbon nanotubes, Sensor. Actuator. B Chem. 354 (2022) 131216, https://doi.org/10.1016/j.snb.2021.131216.
[33] A.C. Schmidt, X. Wang, Y. Zhu, L.A. Sombers, Carbon nanotube yarn electrodes for enhanced detection of neurotransmitter dynamics in live brain tissue, ACS Nano 7 (2013) 7864–7873, https://doi.org/10.1021/nn402857u.
[34] E. Pitzalis, R. Psaro, C. Evangelisti, From metal vapor to supported single atoms, clusters and nanoparticles: recent advances to heterogeneous catalysts, Inorg. Chim. Acta. 533 (2022) 120782, https://doi.org/10.1016/j.ica.2021.120782.
[35] M. Marelli, A. Jouve, A. Villa, R. Psaro, A. Balerna, L. Prati, C. Evangelisti, Hybrid Au/CuO nanoparticles: effect of structural features for selective benzyl alcohol oxidation, J. Phys. Chem. C 123 (2019) 2864–2871, https://doi.org/10.1021/acs.jpcc.8b09449.
[36] W. Oberhauser, C. Evangelisti, M. Marelli, V.D. Santo, C. Cepek, M. Bellini, Gold nanoparticles onto cerium oxycarbonate as highly efficient catalyst for aerobic allyl alcohol oxidation, Catal. Commun. 140 (2020) 105989, https://doi.org/10.1016/j.catcom.2020.105989.
[37] A. Jouve, G. Nagy, F. Somodi, C. Tiozzo, A. Villa, A. Balerna, A. Beck, C. Evangelisti, L. Prati, Gold-silver catalysts: effect of catalyst structure on the selectivity of glycerol oxidation, J. Catal. 368 (2018) 324–335, https://doi.org/10.1016/j.jcat.2018.10.019.
[38] C. Evangelisti, E. Schiavi, L.A. Aronica, R. Psaro, A. Balerna, G. Martra, Solvated metal atoms in the preparation of supported gold catalysts. https://api.semanticscholar.org/CorpusID:99448160, 2015.
[39] M. Bellini, M.G. Folliero, C. Evangelisti, Q. He, Y. Hu, M. V Pagliaro, W. Oberhauser, A. Marchionni, J. Filippi, H.A. Miller, F. Vizza, A gold–palladium nanoparticle alloy catalyst for CO production from CO2 electroreduction, Energy Technol. 7 (2019) 1800859, https://doi.org/10.1002/ente.201800859.
[40] M.C. Biesinger, Accessing the robustness of adventitious carbon for charge referencing (correction) purposes in XPS analysis: insights from a multi-user facility data review, Appl. Surf. Sci. 597 (2022) 153681, https://doi.org/10.1016/j.apsusc.2022.153681.
[41] T. Shahar, N. Tal, D. Mandler, The synthesis and characterization of thiol-based aryl diazonium modified glassy carbon electrode for the voltammetric determination of low levels of Hg(II), J. Solid State Electrochem. 17 (2013) 1543–1552, https://doi.org/10.1007/s10008-013-2009-3.
[42] G. Moro, A. Silvestri, A. Ulrici, F. Conzuelo, C. Zanardi, How to optimize the analytical performance of differential pulse voltammetry: one variable at time versus Design of Experiments, J. Solid State Electrochem. 28 (2024) 1403–1415, https://doi.org/10.1007/s10008-023-05753-x.
[43] J.L. Bahr, J.M. Tour, Covalent chemistry of single-wall carbon nanotubes, J. Mater. Chem. 12 (2002) 1952–1958, https://doi.org/10.1039/B201013P.
[44] C. Wetzl, A. Silvestri, M. Garrido, H.-L. Hou, A. Criado, M. Prato, The covalent functionalization of surface-supported graphene: an update, Angew. Chem. Int. Ed. 62 (2023) e202212857, https://doi.org/10.1002/anie.202212857.
[45] Z. Peng, A.H. Holm, L.T. Nielsen, S.U. Pedersen, K. Daasbjerg, Covalent sidewall functionalization of carbon nanotubes by a "Formation−Degradation" approach, Chem. Mater. 20 (2008) 6068–6075, https://doi.org/10.1021/cm800954t.
[46] H.J. Salavagione, J. Sherwood, M. De bruyn, V.L. Budarin, G.J. Ellis, J.H. Clark, P. S. Shuttleworth, Identification of high performance solvents for the sustainable processing of graphene, Green Chem. 19 (2017) 2550–2560, https://doi.org/10.1039/C7GC00112F.
[47] High Resolution XPS of Organic Polymers: The Scienta ESCA300 Database, G. Beamson, D. Briggs, J. Chem. Educ. 70 (1993) A25, https://doi.org/10.1021/ed070pA25.5.
[48] A. Silvestri, A. Criado, F. Poletti, F. Wang, P. Fanjul-Bolado, M.B. González-García, C. García-Astrain, L.M. Liz-Marzán, X. Feng, C. Zanardi, M. Prato, Bioresponsive, electroactive, and inkjet-printable graphene-based inks, Adv. Funct. Mater. 32 (2022) 2105028, https://doi.org/10.1002/adfm.202105028.
[49] B. Daou, A. Silvestri, H. Lasa, D. Mancino, M. Prato, N. Alegret, Organic functional group on carbon nanotube modulates the maturation of SH-SY5Y neuronal models, Macromol. Biosci. 23 (2023) 2300173, https://doi.org/10.1002/mabi.202300173.
[50] M.P. Casaletto, A. Longo, A. Martorana, A. Prestianni, A.M. Venezia, XPS study of supported gold catalysts: the role of Au0 and Au+δ species as active sites, Surf. Interface Anal. 38 (2006) 215–218, https://doi.org/10.1002/sia.2180.
[51] A. Silvestri, S. Vázquez-Díaz, G. Misia, F. Poletti, R. López-Domene, V. Pavlov, C. Zanardi, A.L. Cortajarena, M. Prato, An electroactive and self-assembling bio-ink, based on protein-stabilized nanoclusters and graphene, for the manufacture of fully inkjet-printed paper-based analytical devices, Small n/a (2023) 2300163, https://doi.org/10.1002/smll.202300163.
[52] A.Yu Vasil'kov, A. V Naumkin, I.O. Volkov, V.L. Podshibikhin, G. V Lisichkin, A. R. Khokhlov, XPS/TEM characterisation of Pt-Au/C cathode electrocatalysts prepared by metal vapour synthesis, Surf. Interface Anal. 42 (2010) 559–563, https://doi.org/10.1002/sia.3269.
[53] B.E. Hayden, Particle size and support effects in electrocatalysis, Acc. Chem. Res. 46 (2013) 1858–1866, https://doi.org/10.1021/ar400001n.
[54] P. Suchomel, L. Kvitek, R. Prucek, A. Panacek, A. Halder, S. Vajda, R. Zboril, Simple size-controlled synthesis of Au nanoparticles and their size-dependent catalytic activity, Sci. Rep. 8 (2018) 4589, https://doi.org/10.1038/s41598-018-22976-5.
[55] E. Romanovskaia, P. Slovenský, S.M. Kalantarian, L. Laundry-Mottiar, V. Romanovski, M. Halama, M. Auinger, Y.S. Hedberg, Electrochemical estimations of the gold nanoparticle size effect on cysteine-gold oxidation, J. Electrochem. Soc. 169 (2022) 021501, https://doi.org/10.1149/1945-7111/ac4bf8.
[56] R.A. Masitas, F.P. Zamborini, Oxidation of highly unstable <4 nm diameter gold nanoparticles 850 mV negative of the bulk oxidation potential, J. Am. Chem. Soc. 134 (2012) 5014–5017, https://doi.org/10.1021/ja2108933.
[57] K.J. Lee, N. Elgrishi, B. Kandemir, J.L. Dempsey, Electrochemical and spectroscopic methods for evaluating molecular electrocatalysts, Nat. Rev. Chem 1 (2017) 39, https://doi.org/10.1038/s41570-017-0039.
[58] K. Khoshnevisan, H. Maleki, E. Honarvarfard, H. Baharifar, M. Gholami, F. Faridbod, B. Larijani, R. Faridi Majidi, M.R. Khorramizadeh, Nanomaterial based electrochemical sensing of the biomarker serotonin: a comprehensive review, Microchim. Acta 186 (2019) 49, https://doi.org/10.1007/s00604-018-3069-y.
[59] F.R. Simões, M.G. Xavier, 6 - electrochemical sensors, in: A.L. Da Róz, M. Ferreira, F. de Lima Leite, O.N. Oliveira (Eds.), Nanoscience and its Applications, William Andrew Publishing, 2017, pp. 155–178, https://doi.org/10.1016/B978-0-323-49780-0.00006-5.
[60] S. Shahrokhian, L. Fotouhi, Carbon paste electrode incorporating multi-walled carbon nanotube/cobalt salophen for sensitive voltammetric determination of tryptophan, Sensor. Actuator. B Chem. 123 (2007) 942–949, https://doi.org/10.1016/j.snb.2006.10.053.
[61] A.A. Ensafi, K. Zarei, T. Khayamian, Determination of ultratrace amounts of ruthenium by differential pulse voltammetry using factorial design for optimization, Microchem. J. 63 (1999) 235–242, https://doi.org/10.1006/mchj.1999.1786.
[62] K. Eersels, P. Lieberzeit, P. Wagner, A review on synthetic receptors for bioparticle detection created by surface-imprinting techniques—from principles to applications, ACS Sens. 1 (2016) 1171–1187, https://doi.org/10.1021/acssensors.6b00572.
[63] A. Berni, A. Ait Lahcen, K.N. Salama, A. Amine, 3D-porous laser-scribed graphene decorated with overoxidized polypyrrole as an electrochemical sensing platform for dopamine, J. Electroanal. Chem. 919 (2022) 116529, https://doi.org/10.1016/j.jelechem.2022.116529.
[64] S.E. Elugoke, A.S. Adekunle, O.E. Fayemi, E.D. Akpan, B.B. Mamba, E.-S.M. Sherif, E.E. Ebenso, Molecularly imprinted polymers (MIPs) based electrochemical sensors for the determination of catecholamine neurotransmitters – review, Electrochemical Science Advances 1 (2021) e2000026, https://doi.org/10.1002/elsa.202000026.
[65] E. Costa-Rama, M.T. Fernández Abedul, Chapter 5 - adsorptive stripping voltammetry of indigo blue in a flow system, in: M.T. Fernandez Abedul (Ed.), Laboratory Methods in Dynamic Electroanalysis, Elsevier, 2020, pp. 47–56, https://doi.org/10.1016/B978-0-12-815932-3.00005-X.